Commun. Comput. Phys.
doi: 10.4208/cicp.150313.171013s

Vol. **15**, No. 4, pp. 1045-1067
April 2014

Immersed Finite Element Method for Interface Problems with Algebraic Multigrid Solver

Wenqiang Feng[1], Xiaoming He[1,*], Yanping Lin[2,3] and Xu Zhang[4]

[1] *Department of Mathematics and Statistics, Missouri University of Science and Technology, Rolla, MO 65409, USA.*
[2] *Department of Applied Mathematics, Hong Kong Polytechnic University, Hung Hom, Hong Kong.*
[3] *Department of Mathematical and Statistics Science, University of Alberta, Edmonton, AB, T6G 2G1, Canada.*
[4] *Department of Mathematics, Virginia Tech, Blacksburg, VA 24061, USA.*

Received 15 March 2013; Accepted (in revised version) 17 October 2013

Available online 21 January 2014

Abstract. This article is to discuss the bilinear and linear immersed finite element (IFE) solutions generated from the algebraic multigrid solver for both stationary and moving interface problems. For the numerical methods based on finite difference formulation and a structured mesh independent of the interface, the stiffness matrix of the linear system is usually not symmetric positive-definite, which demands extra efforts to design efficient multigrid methods. On the other hand, the stiffness matrix arising from the IFE methods are naturally symmetric positive-definite. Hence the IFE-AMG algorithm is proposed to solve the linear systems of the bilinear and linear IFE methods for both stationary and moving interface problems. The numerical examples demonstrate the features of the proposed algorithms, including the optimal convergence in both L^2 and semi-H^1 norms of the IFE-AMG solutions, the high efficiency with proper choice of the components and parameters of AMG, the influence of the tolerance and the smoother type of AMG on the convergence of the IFE solutions for the interface problems, and the relationship between the cost and the moving interface location.

AMS subject classifications: 65F10, 65N30, 35J15, 35K20

Key words: Interface problems, immersed finite elements, algebraic multigrid method.

1 Introduction

In this article, we first consider the following second order elliptic interface problem:

*Corresponding author. *Email addresses:* fw253@mst.edu (W. Feng), hex@mst.edu (X. He), yanlin@ualberta.ca (Y. Lin), xuz@vt.edu (X. Zhang)

$$\begin{cases} -\nabla\cdot\big(\beta\nabla u\big)=f(X), & X\in\Omega, \\ u(X)=g(X), & X\in\partial\Omega, \end{cases} \tag{1.1}$$

together with the jump conditions on the interface Γ:

$$[u]|_\Gamma=0, \tag{1.2a}$$

$$\Big[\beta\frac{\partial u}{\partial\mathbf{n}}\Big]\Big|_\Gamma=0. \tag{1.2b}$$

Here, see Fig. 1, without loss of generality, we consider the case in which $\Omega\subset IR^2$ is an open rectangular domain, and the interface curve Γ is defined by a smooth function which separates Ω into two sub-domains Ω^-, Ω^+ such that $\overline{\Omega}=\overline{\Omega^-}\cup\overline{\Omega^+}\cup\Gamma$, and the coefficient $\beta(X)$ is a positive piecewise constant function defined by

$$\beta(X)=\begin{cases} \beta^-, & X\in\Omega^-, \\ \beta^+, & X\in\Omega^+. \end{cases}$$

We will also consider the following parabolic moving interface problem:

$$\begin{cases} u_t-\nabla\cdot(\beta\nabla u)=f(t,X), & X\in\Omega, \quad t\in(0,T_{end}], \\ u(t,X)=g(t,X), & X\in\partial\Omega, \quad t\in(0,T_{end}], \\ u(0,X)=u_0(X), & X\in\overline{\Omega}, \end{cases} \tag{1.3}$$

with the jump condition on a moving interface $\Gamma(t)$:

$$[u]|_{\Gamma(t)}=0, \tag{1.4a}$$

$$\Big[\beta\frac{\partial u}{\partial\mathbf{n}}\Big]\Big|_{\Gamma(t)}=0. \tag{1.4b}$$

Without loss of generality, we consider the case in which the interface curve $\Gamma(t)$ is defined by a smooth function $\Gamma:[0,T_{end}]\to\Omega$. At any time $t\in[0,T_{end}]$, the interface $\Gamma(t)$ separates Ω into two sub-domains $\Omega^+(t)$ and $\Omega^-(t)$ such that $\Omega=\Omega^+(t)\cup\Omega^-(t)\cup\Gamma(t)$ and $\Gamma(t)\cap\partial\Omega=\emptyset$. The coefficient function $\beta(t,X)$ is discontinuous across the interface $\Gamma(t)$. For simplicity, we assume $\beta(t,X)$ is a piece-wise constant function as follows:

$$\beta(t,X)=\begin{cases} \beta^-, & X\in\Omega^-(t), \\ \beta^+, & X\in\Omega^+(t). \end{cases}$$

The stationary interface problems (1.1)-(1.2b) and the moving interface problem (1.3)-(1.4b) are involved in many applications of engineering and sciences, such as the field injection problem [25, 77], flow problem [3, 15], electromagnetic problems [4, 8, 43], shape/toplogy optimization problem [7, 19], and the Stefan problem [11, 62]. These interface problems can be solved by conventional finite difference or finite element methods with optimal convergence if a body-fitting mesh is utilized [5, 6, 9, 14, 38]. However,

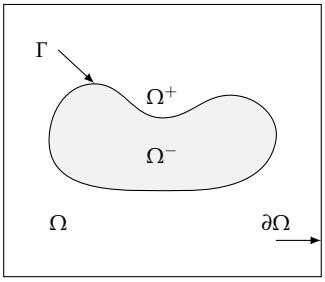

Figure 1: The sketch of domain Ω with the interface Γ.

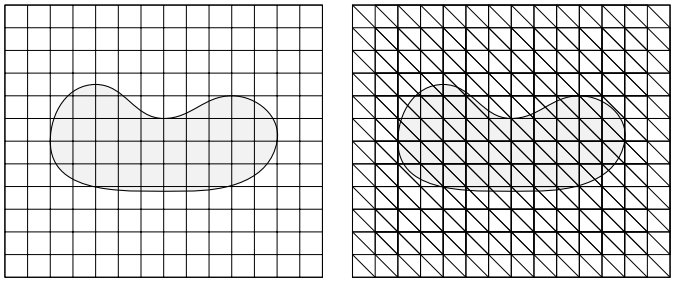

Figure 2: Rectangular and triangular Cartesian meshes independent of the interface.

there are many applications, such as Particle-In-Cell method for plasma particle simulation [44, 60, 61, 71, 72] and moving interface problems [37], in which a structured mesh independent of the interface is preferred for solving the interface problems.

Therefore, many efforts have been attempted to develop numerical methods for solving interface problems on structured meshes (Fig. 2) independent of the interface even if their geometries are non-trivial. In the finite difference formulation, the immersed boundary method [28,45,55,63,64], immersed interface method [21–23,50,68,76], matched interface and boundary method [24, 78–81], cut-cell method [40, 41], and embedded boundary method [39, 42] have been developed.

In real world applications, we often need to solve large scale linear systems arising from these methods many times due to various realistic needs, such as the curse of the dimensionality, the high accuracy requirement, and moving interface. This demands very efficient solvers. The multigrid methods, which are well known for their efficiency and natural preconditioning feature, perform efficiently on Cartesian meshes which can be naturally provided by the aforementioned methods for interface problems. L. Adams and Z. Li [49] designed a geometric multigrid method for the immersed interface method of the second order elliptic interface problems. L. Adams and T. P. Chartier [47] developed a new restriction operator and the corresponding interpolation operator to guarantee that the coarse-grid matrices are *M*-matrices. R. D. Guy and B. Philip discussed a multigrid method for an implicit immersed boundary equations [29]. Moreover, T. Chen and J. Strain [13] developed a Krylov-accelerated multigrid approach to a new piecewise-

polynomial method for elliptic problems with complex interfaces. L. Adams and T. P. Chartier [48] also utilized a similar idea in [47] to design the corresponding algebraic multigrid method and compare it with the geometric one.

For the algebraic multigrid method [65, 67], extra efforts are usually needed in order to design efficient multigrid solvers to solve the non-symmetric linear systems arising from the methods based on finite difference formulation and a structured mesh independent of the interface. On the other hand, the immersed finite element (IFE) methods [1, 2, 10, 16–18, 20, 26, 27, 30–37, 43, 46, 51–54, 56–59, 66, 70, 73–75], which are developed under the general framework of finite elements and proposed by using local basis functions according to the interface jump conditions while their meshes do not have to be aligned with interfaces, naturally provide symmetric positive-definite matrices for the above interface problems. While minimizing the extra efforts to modify the traditional finite element packages, the IFE methods can also easily deal with complex interface with optimal accuracy order. Hence we believe that the combination of the features of the algebraic multigrid method (such as its efficiency, preconditioning capability and independence of the geometry) and the features of the IFE methods (such as their symmetric positive-definite matrices, capability to handle the interface without using body-fitting meshes, and optimal convergence rates) can generate very efficient and competitive numerical methods for large-scale applications in which a structured mesh independent of the interface is preferred for solving the interface problems.

The rest of this article is organized as follows. In Section 2, we recall the definitions of the bilinear and 2D linear IFE spaces. In Section 3, we first combine the algebraic multigrid method with the IFE method for the elliptic interface problem, and then we extend the resulted algorithm to a Crank-Nicolson-type IFE method for the parabolic moving interface problem. In Section 4, we present some numerical examples to illustrate the features of IFE-AMG algorithms. Finally, we summarize our results in Section 5.

2 The bilinear and 2D linear immersed finite elements

In this section, we briefly recall the bilinear IFE space [31, 56] and the 2D linear IFE space [53, 54].

First, we consider a rectangular Cartesian mesh (see the left graph of Fig. 2) independent of the interface. Let $\mathcal{T}_h$ denote the collection of all elements in a mesh with parameter h. When h is small enough, most of elements in $\mathcal{T}_h$ are non-interface elements not intersecting with the interface Γ. Only those elements in the vicinity of Γ have the possibility to be cut through by Γ and become the so-called interface elements. We will use $\mathcal{T}_{int}$ to denote the collection of all interface elements of $\mathcal{T}_h$.

On each non-interface element T, we let the local finite element space $S_h(T)$ be $S_h^{non}(T)$, which is spanned by the four standard bilinear nodal basis functions $\psi_i(x,y)$, $i=1,2,3,4$ on T. To describe the local IFE space on an interface element $T\in\mathcal{T}_{int}$, we assume that the vertices of T are A_i, $i=1,2,3,4$, with $A_i=(x_i,y_i)^T$. Without loss of generality,

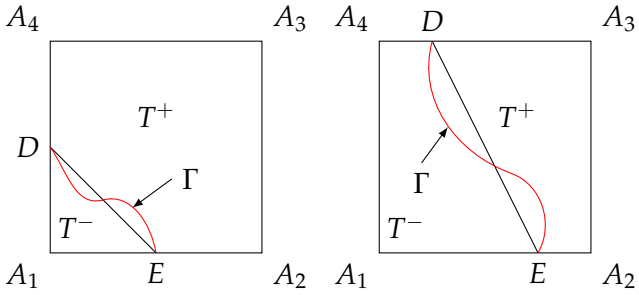

Figure 3: Two typical rectangular interface elements. The element on the left is of Type I while the one on the right is of Type II.

we assume that ∂T intersects with Γ at two points $D=(x_D,y_D)^T$ and $E=(x_E,y_E)^T$. When the mesh is fine enough, there are two types of rectangle interface elements. Type I are those for which the interface intersects with two of its adjacent edges; Type II are those for which the interface intersects with two of its opposite edges, see the sketches in Fig. 3.

Since the line $\overline{DE}$ separates T into two subsets T^- and T^+, we naturally form a piecewise function by two bilinear polynomials defined in T^- and T^+, respectively. Then by using the interface conditions (1.2a)-(1.2b), the bilinear immersed functions are defined as follows [31,56]:

$$\psi(x,y)=\begin{cases} \psi^-(x,y)=a^-x+b^-y+c^-+d^-xy, & (x,y)\in T^-,\\ \psi^+(x,y)=a^+x+b^+y+c^++d^+xy, & (x,y)\in T^+,\\ \psi^-(D)=\psi^+(D),\ \psi^-(E)=\psi^+(E),\ d^-=d^+, & \\ \int_{\overline{DE}}\Big(\beta^-\dfrac{\partial\psi^-}{\partial\mathbf{n}_{\overline{DE}}}-\beta^+\dfrac{\partial\psi^+}{\partial\mathbf{n}_{\overline{DE}}}\Big)ds=0. & \end{cases} \tag{2.1}$$

Now let $\psi_i(X)$ be the bilinear IFE function described by (2.1) such that

$$\psi_i(x_j,y_j)=\begin{cases} 1, & \text{if } i=j,\\ 0, & \text{if } i\neq j, \end{cases}$$

for $1\le i,j\le 4$, and we call them the bilinear IFE nodal basis functions on an interface element T. We then let $S_h^{int}(T)=span\{\psi_i, i=1,2,3,4\}$.

In summery, for each element $T\in\mathcal{T}_h$, we define

$$S_h(T)=\begin{cases} S_h^{non}(T), & \text{if } T \text{ is a non-interface element},\\ S_h^{int}(T), & \text{if } T \text{ is an interface element}. \end{cases}$$

Let $\mathcal{N}_h=\{X_i\}_{i=1}^N$ denote the set of nodes in $\mathcal{T}_h$, $\mathcal{N}_h^o=\mathcal{N}_h\cap\Omega$, $\mathcal{N}_h^b=\mathcal{N}_h\cap\partial\Omega$, $\mathcal{I}_h^o=\{i:X_i\in\mathcal{N}_h^o\}$, and $\mathcal{I}_h^b=\{i:X_i\in\mathcal{N}_h^b\}$. Define $\phi_i(X)$ $(i=1,\cdots,N)$ to be a piecewise bilinear function such that

$$\phi_i|_T\in S_h(T),\quad \forall T\in\mathcal{T}_h \quad\text{and}\quad \phi_i(X_j)=\delta_{ij},\quad \forall X_j\in\mathcal{N}_h.$$

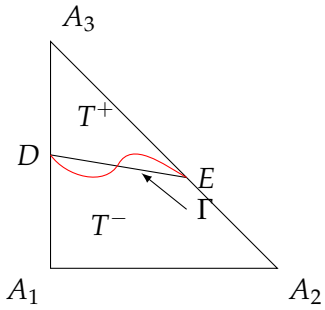

Figure 4: A typical triangular interface element.

Then the bilinear IFE space on the whole domain Ω is defined as

$$S_h^{IFE}(\Omega)=span\{\phi_i(X):1\le i\le N\}.$$

We also define the subspace $S_{h,0}^{IFE}(\Omega)\subset S_h^{IFE}(\Omega)$ such that

$$S_{h,0}^{IFE}(\Omega)=span\{\phi_i(X):i\in\mathcal{I}_h^o\}.$$

Remark 2.1. Here $\phi_i(X)$ is a global bilinear IFE basis function if X_i is a node of any interface element. Otherwise, $\phi_i(X)$ is a standard global bilinear finite element basis function associated with the node X_i. Since IFE functions are discontinuous on the element edges cut by the interface, the immersed finite elements are nonconforming [31,56].

In the following we consider a triangular Cartesian mesh (see the right graph in Fig. 2) independent of the interface. On each of the non-interface element T, we let the local finite element space $S_h(T)$ be $S_h^{non}(T)$ spanned by the three standard linear nodal basis functions $\phi_i(x,y)$, $i=1,2,3$ on T. For an interface element T with vertices $A_i=(x_i,y_i)^T$, $i=1,2,3$, without loss of generality, we assume that ∂T intersects with Γ at two points $D=(x_D,y_D)^T$ and $E=(x_E,y_E)^T$. There is only one type of triangle interface elements, see the sketch in Fig. 4.

Then by using the interface conditions (1.2a)-(1.2b), a typical 2D linear immersed finite element function is defined as follows [53,54]:

$$\psi(x,y)=\begin{cases}\psi^-(x,y)=a^-x+b^-y+c^-, & (x,y)\in T^-,\\ \psi^+(x,y)=a^+x+b^+y+c^+, & (x,y)\in T^+,\\ \psi^-(D)=\psi^+(D),\ \psi^-(E)=\psi^+(E), & \\ \beta^-\dfrac{\partial\psi^-}{\partial\mathbf{n}_{\overline{DE}}}-\beta^+\dfrac{\partial\psi^+}{\partial\mathbf{n}_{\overline{DE}}}=0, & \end{cases}\tag{2.2}$$

where $\mathbf{n}_{\overline{DE}}$ is the unit vector perpendicular to the line $\overline{DE}$. We let $\psi_i(X)$ be the linear IFE function described by (2.2) such that

$$\psi_i(x_j,y_j)=\begin{cases}1, & \text{if } i=j,\\ 0, & \text{if } i\neq j,\end{cases}$$

for $1 \le i,j \le 3$, and we call them the 2D linear IFE nodal basis functions on an interface element T. We then let $S_h^{int}(T) = span\{\phi_i,\ i=1,2,3\}$. Then we can use the same way as in the bilinear IFE space to define $S_h(T)$, $\phi_i(X)$, $S_h^{IFE}(\Omega)$ and $S_{h,0}^{IFE}(\Omega)$ for the 2D linear IFE space.

3 The IFE-AMG algorithm

In this section we will first describe how to use the IFE function spaces and the algebraic multigrid method to solve the elliptic interface problems. And then we will apply the same idea to a Crank-Nicolson-type IFE method for the parabolic moving interface problem.

To formulate the linear system arising from the IFE method for the elliptic interface problem, we will first briefly recall the weak formulation and the IFE formulation [35,54, 56]. The weak formulation for the elliptic interface problem is to find $u \in H^1(\Omega)$ such that

$$\begin{aligned} &\int_\Omega \beta \nabla u \cdot \nabla v dxdy = \int_\Omega f v dxdy, && \forall v \in H_0^1(\Omega), \\ &u(X) = g(X), && X \in \partial\Omega. \end{aligned}$$

Then the IFE formulation is to find $u_h \in S_h^{IFE}(\Omega)$ such that

$$\sum_{T\in\mathcal{T}_h} \int_T \beta \nabla u_h \cdot \nabla v_h dxdy = \sum_{T\in\mathcal{T}_h} \int_T f v_h dxdy, \quad \forall v_h \in S_{h,0}^{IFE}(\Omega), \tag{3.1a}$$

$$u_h(X) = g(X), \quad X \in \mathcal{N}_h^b. \tag{3.1b}$$

Based on the construction of the IFE space $S_h^{IFE}(\Omega)$ and the given Dirichlet boundary condition, the approximate solution to the elliptic interface problem (1.1)-(1.2b) is taken in the following form:

$$u_h(X) = \sum_{k\in\mathcal{I}_h^o} u_k \phi_k(X) + \sum_{s\in\mathcal{I}_h^b} g(X_s)\phi_s(X). \tag{3.2}$$

Rewriting the above system in matrix formulation yields

$$A_h \vec{u}_h = \vec{b}_h, \tag{3.3}$$

where

- $A_h = (a_{ij})_{n\times n}$ is the stiffness matrix with

$$a_{ij} = \sum_{T\in\mathcal{T}_h} \int_T \beta \nabla \phi_{k_i} \cdot \nabla \phi_{k_j} dX.$$

- $\vec{b}_h=(b_i)_{n\times 1}$ is the source vector with

$$b_i=\sum_{T\in\mathcal{T}_h}\int_T \phi_{k_i} f dX-\sum_{s\in\mathcal{I}_h^b}\Big(\sum_{T\in\mathcal{T}_h}\int_T \beta\nabla\phi_{k_i}\cdot\nabla\phi_s dX\Big)g(X_s).$$

- $\vec{u}_h=(u_{k_i})_{n\times 1}$ is the unknown vector.

Remark 3.1. It is straightforward to see that the stiffness matrix A_h arising from the IFE method is symmetric positive definite, which is critical to the algebraic multigrid method. The optimal convergence rates are also expected for the IFE solutions u_h, which are second order in L^2 norm and first order in H^1 semi-norm for the linear and bilinear IFEs. The numerical experiments in the next section will verify this expectation.

In the following we will introduce the AMG method [12,65,69] that is appropriate for solving the linear system (3.3) which arises from the IFE method. Let $A_h^1=A_h$, $\vec{u}_h^1=\vec{u}_h$, $\vec{b}_h^1=\vec{b}_h$. Then in one V-cycle a sequence of linear systems

$$A_h^m\vec{u}_h^m=\vec{b}_h^m,\quad m=1,\cdots,M,$$

can be generated from different grid levels. Here $A_h^m=(a_{ij}^m)_{n_m\times n_m}$, $\vec{b}_h=(b_i^m)_{n_m\times 1}$, $\vec{u}_h=(u_i^m)_{n_m\times 1}$, and $n=n_1>n_2>\cdots>n_m$. Now we discuss two main phases of the AMG algorithm: setup phase and solution phase [12].

In the setup phase, let Ω^m denote the set of unknowns u_i^m $(1\le i\le n_m)$ of the m^{th} grid level. And the coarser grid Ω^{m+1} is chosen as a subset of Ω^m, which is denoted as C^m in the m^{th} grid level. The remaining subset Ω^m-C^m will be denoted by F^m. A point u_i^m is said to be strongly connected to u_j^m provided there exists a positive constant (the strong connection threshold) $\eta\in(0,1]$ such that

$$|a_{ij}^m|\ge\eta\cdot\max_{\substack{k\neq s\\ 1\le k,s\le n_m}}|a_{ks}^m|,\quad 0<\eta\le 1. \tag{3.4}$$

Let S_i^m denote the set of all strongly connected points of u_i^m and let the coarse interpolatory set be $C_i^m=C^m\cap S_i^m$. In general, C^m and F^m are chosen by the following criteria:

(C1) For each $u_i^m\in F^m$, each point $u_j^m\in S_i^m$ should be either in C_i^m itself or should be strongly connected to at least one point in C_i^m.

(C2) C^m should be the subset of all points with the property that no two coarse points are strongly connected to each other.

Define the set of points which are strongly connected to u_i^m to be

$$S_i^{m,T}\equiv\{u_j^m:\ u_i^m\in S_j^m\}. \tag{3.5}$$

For a set P, let $|P|$ denote the number of the elements in P. Then Algorithm 3.1 is proposed by Ruge and Stüben in [65,67] can be used to chose the coarse grid $\Omega^{m+1}=C^m$ and F^m.

Algorithm 3.1. The construction of coarse grid.

Input: Ω^m.
Output: C^m and F^m.
Method:

$C^m \leftarrow \emptyset$, $F^m \leftarrow \emptyset$, $\vec{u}_h^m \leftarrow \Omega^m$ and $\lambda_k^m = |S_k^{m,T}|$ $(1 \le k \le n_m)$
for $(1 \le i \le n_m)$ **do**
  if $(\vec{u}_h^m \neq \emptyset)$ **then**
    Pick the $u_i^m \in \vec{u}_h^m$ such that $\lambda_i^m = \max_{1\le k\le n_m} \lambda_k^m$, and set

$$C^m = C^m \cup \{u_i^m\}, \quad \vec{u}_h^m = \vec{u}_h^m - \{u_i^m\}$$

    for (all $u_j^m \in S_i^{m,T} \cap \vec{u}_h^m$) **do**
      Set $F^m = F^m \cup \{j\}$ and $\vec{u}_h^m = \vec{u}_h^m - \{j\}$
      for (all $u_l^m \in S_j^m \cap \vec{u}_h^m$) **do**
        set $\lambda_l^m = \lambda_l^m + 1$
      end for
    end for
    for (all $u_j^m \in S_i^m \cap \vec{u}_h^m$) **do**
      set $\lambda_j^m = \lambda_j^m - 1$
    end for
  else
    Stop.
  end if
end for

Once the coarse grid Ω^{m+1} is chosen, the interpolation operators I_{m+1}^m, restriction operators I_m^{m+1} and the coarse grid equation can be constructed as follows. Let $N_i^m = \{u_j^m \in \Omega^m : j \neq i,\ a_{ij}^m \neq 0\}$ denote the neighborhood of a point $u_i^m \in \Omega^m$, and $D_i^m = N_i^m - C_i^m$. Then the set of the fine grid neighborhood points which are strongly connected to u_i^m will be $D_i^{m,s} = D_i^m \cap S_i^m$, and the rest set of the neighborhood points which are weakly connected (not strongly connected) to u_i^m will be $D_i^{m,w} = D_i^m - D_i^{m,s}$. Each $u_i^m \in C^m$ can be directly interpolated from the corresponding variable in Ω^{m+1} with unity weight. Each $u_i^m \in F^m$ can be interpolated as a weighted summation of the points in the coarse interpolatory set C_i^m. Assume $u_i^m \in C^m$ is corresponding to $u_{k_i}^{m+1} \in \Omega^{m+1}$. Ruge and Stüben proposed the corresponding interpolation formula [65]:

$$I_{m+1}^m \{u_k^{m+1}\}_{k=1}^{n_{m+1}} = \begin{cases} u_{k_i}^{m+1}, & \forall u_i^m \in C^m, \\ \sum_{\{j:u_j^m \in C_i^m\}} w_{ij}^m u_{k_j}^{m+1}, & \forall u_i^m \in F^m, \end{cases} \tag{3.6}$$

where

$$w_{ij}^m = -\frac{1}{a_{ii}^m + \sum_{\{r:u_r^m \in D_i^{m,w}\}} a_{ir}^m} \left[a_{ij}^m + \frac{\sum_{\{r:u_r^m \in D_i^{m,s}\}} a_{ir}^m a_{rj}^m}{\sum_{\{l:u_l^m \in C_i^m\}} a_{il}^m} \right]. \tag{3.7}$$

The Galerkin type method in [65] is a simple approach to define the restriction operator I_m^{m+1}

$$I_m^{m+1} = (I_{m+1}^m)^T \tag{3.8}$$

and

$$A_h^{m+1} = I_m^{m+1} A_h^m I_{m+1}^m, \quad \vec{b}_h^{m+1} = I_m^{m+1} \vec{b}_h^m I_{m+1}^m.$$

In the solution phase, the smoothing operator needs to be chosen with proper parameters ν_1 and ν_2, which are the number of the pre-smoothing and post-smoothing steps. In the next section, we will investigate the influence of the type of the operator (Gauss-Seidel and incomplete LU) and these two parameters. Furthermore, we will consider V-cycle only with the maximum number of levels M in this article. Another critical component of AMG is the stopping tolerance, which may have significant effect on the accuracy. Our study in the next section shows that the tolerance needs to be small enough for the chosen mesh size. Once all the above components are specified, the recursively defined IFE-AMG algorithm (Algorithm 3.2) with V-cycle can be proposed in the usual framework as follows [65].

Algorithm 3.2. The IFE-AMG algorithm of the elliptic interface problem.

Input: Model parameters and AMG parameters.
Output: IFE-AMG approximation solution $\vec{u}_h$.
Method:

1: Assemble the matrix from the IFE formulation: $A_h = (a_{ij})_{n\times n}$ with $a_{ij} = \sum_{T\in\mathcal{T}_h} \int_T \beta \nabla\phi_{k_i} \cdot \nabla\phi_{k_j} dX$, where $\phi_{k_i}, \phi_{k_j} \in S_{h,0}^{IFE}(\Omega)$
2: Assemble the vector from the IFE formulation: $\vec{b}_h = (f_i)_{n\times 1}$ with $f_i = \sum_{T\in\mathcal{T}_h} \int_T \phi_{k_i} f dX - \sum_{s\in\mathcal{I}_h^b} (\sum_{T\in\mathcal{T}_h} \int_T \beta \nabla\phi_{k_i} \cdot \nabla\phi_s dX) g(X_s)$, where $\phi_{k_i} \in S_{h,0}^{IFE}(\Omega)$ and $\phi_s \in S_h^{IFE}(\Omega)$
3: relative residual$=1$, $\vec{u}_h = 0$
4: **while** relative residual$>$tolerance **do**
5: $m=1$, $A_h^1 = A_h$, $\vec{b}_h^1 = \vec{b}_h$, $\vec{u}_h^1 = \vec{u}_h$
6: Call algorithm $MG(A_h^m, \vec{u}_h^m, \vec{b}_h^m, \Omega^m, \nu_1, \nu_2, m)$ as follows:
7: Call Algorithm 3.1 with Ω^m to obtain the C^m and F^m
8: Set $\Omega^{m+1} = C^m$
9: Define I_{m+1}^m, $I_m^{m+1} = (I_{m+1}^m)^T$
10: Pre-smooth: $\vec{u}_h^m := \text{smooth}(A_h^m, \vec{u}_h^m, \vec{b}_h^m, \nu_1)$
11: Residual: $\vec{r}_h^m = \vec{b}_h^m - A_h^m \vec{u}_h^m$
12: Coarsening: $\vec{r}_h^{m+1} = I_m^{m+1} r^m$, $A_h^{m+1} = I_m^{m+1} A_h^m I_{m+1}^m$, $\vec{b}_h^{m+1} = I_m^{m+1} \vec{b}_h^m I_{m+1}^m$
13: If $m = M$
14: Solve: $A_h^{m+1} \delta^{m+1} = \vec{r}_h^{m+1}$
15: Else
16: Recursion: $\delta^{m+1} = MG(A_h^{m+1}, 0, \vec{r}_h^{m+1}, \Omega^{m+1}, \nu_1, \nu_2, m+1)$
17: EndIf
18: Correction: $\vec{u}_h^m = \vec{u}_h^m + I_{m+1}^m \delta^{m+1} I_m^{m+1}$
19: Post-smooth: $\vec{u}_h^m := \text{smooth}(A_h^m, \vec{u}_h^m, \vec{b}_h^m, \nu_2)$

20: END of MG
21: $\vec{u}_h = \vec{u}_h^1$
22: relative residual $= \|\vec{b}_h - A_h\vec{u}_h\| / \|\vec{b}_h\|$
23: **end while**

Now we discuss the parabolic moving interface problem (1.3)-(1.4b), for which we will utilize a Crank-Nicolson-type IFE method [37] together with the above IFE-AMG algorithm. The matrix formed at each time iteration step will be different from the one from elliptic equation, but still symmetric positive definite.

At any time t, we define $\mathcal{N}_h^{i,t}$ to be the set of nodes of all interface elements at the time t and let $\mathcal{N}_h^{n,t} = \mathcal{N}_h / \mathcal{N}_h^{i,t}$ denote the rest of the nodes. Let $\phi_j^t(X)$ denote the global bilinear or linear IFE basis function, which has been discussed in Section 2, associated with the node $X_j \in \mathcal{N}_h^{i,t}$ at the time t while $\phi_j^t(X)$ is a standard global linear finite element basis function for $X_j \in \mathcal{N}_h^{n,t}$. Then we look for an IFE approximate solution to the parabolic interface problem (1.3)-(1.4b) in the following form:

$$u_h(t,X) = \sum_{X_j \in \mathcal{N}_h} u_j(t)\phi_j^t(X). \tag{3.9}$$

From the above definitions, we know that if $X_j \in \mathcal{N}_h^{i,t}$, then $\phi_j^t(X)$ depends on the interface location, hence depends on the time t. On the other hand, $\phi_j^t(X)$ is independent of the time t for $X_j \in \mathcal{N}_h^{n,t}$. Therefore,

$$\frac{\partial u_h(t,X)}{\partial t} = \sum_{X_j \in \mathcal{N}_h} \frac{\partial u_j(t)}{\partial t}\phi_j^t(X) + \sum_{X_j \in \mathcal{N}_h^{i,t}} u_j(t)\frac{\partial \phi_j^t(X)}{\partial t}. \tag{3.10}$$

Based on the following standard weak form at a given time t:

$$\int_\Omega v\frac{\partial u}{\partial t}dX + \int_\Omega \nabla v \cdot (\beta \nabla u)dX = \int_\Omega vf dX, \quad \forall v \in H_0^1(\Omega),$$

which is equivalent to

$$\sum_{T \in \mathcal{T}_h}\int_T v\frac{\partial u}{\partial t}dX + \sum_{T \in \mathcal{T}_h}\int_T \nabla v \cdot (\beta \nabla u)dX = \int_\Omega vf dX, \quad \forall v \in H_0^1(\Omega),$$

the following system can be obtained from the IFE semi-discretization [37]:

$$M_h(t)\mathbf{u}'(t) + K_h(t)\mathbf{u}(t) + A_h(t)\mathbf{u}(t) = \mathbf{f}(t), \tag{3.11}$$

where

- $M_h(t) = (m_{ij}(t))$ is the mass matrix with $m_{ij} = \int_\Omega \phi_i^t \phi_j^t dX$.

- $K_h(t)=(k_{ij}(t))$ with $k_{ij}=\int_\Omega \phi_i^t \partial\phi_j^t/\partial t dX$.
- $A_h(t)=(a_{ij}(t))$ is the stiffness matrix with $a_{ij}=\int_\Omega \nabla\phi_i^t\cdot(\beta\nabla\phi_j^t)dX$.
- $\mathbf{f}(t)=(f_i(t))$ is the source vector with $f_i(t)=\int_\Omega \phi_i^t f dX$.
- $\mathbf{u}(t)$ is the vector whose entries are $u_j(t)$, i.e., $\mathbf{u}(t)=(u_j(t))$.

For the time discretization, without loss of generality, we use a uniform partition $0=t_0<t_1<\cdots<t_N=T$ in time, where $t_n=n\tau$ with $\tau=T_{end}/N$. Then we look for approximations such that

$$u_h^n(X)=\sum_{X_j\in\mathcal{N}_h} u_j^n\phi_j^{t_n}(X)\approx u_h(t_n,X).$$

In effect, we look for $\vec{u}^n=(u_j^n)\approx\vec{u}(t_n)$, for $n=1,2,\cdots,N$. Then applying the idea of Crank-Nicolson type discretization to (3.11) leads to the following algorithm [37]:

$$\begin{aligned}&\left(M_h^{n+\frac12,n+\frac12}+\frac{\tau}{2}A_h^{n+\frac12,n+\frac12,n+\frac12}+\frac{\tau}{2}K_h^{n+\frac12,n+\frac12}\right)\vec{u}^{n+1}\\ =&\left(M_h^{n+\frac12,n+\frac12}-\frac{\tau}{2}A_h^{n+\frac12,n+\frac12,n+\frac12}-\frac{\tau}{2}K_h^{n+\frac12,n+\frac12}\right)\vec{u}^n+\tau\vec{f}^{n+\frac12,n+\frac12},\end{aligned}\tag{3.12}$$

where

- $M_h^{n_v,n_u}=(m_{ij}^{n_v,n_u})$ is the mass matrix, where $m_{ij}^{n_v,n_u}=\int_\Omega\phi_i^{t_{n_v}}\phi_j^{t_{n_u}}dX$.
- $A_h^{n_\beta,n_v,n_u}=(a_{ij}^{n_\beta,n_v,n_u})$ is the stiffness matrix, where $a_{ij}^{n_\beta,n_v,n_u}=\int_\Omega\nabla\phi_i^{t_{n_v}}\cdot(\beta^{t_{n_\beta}}\nabla\phi_j^{t_{n_u}})dX$.
- $K_h^{n_v,n_u}=(k_{ij}^{n_v,n_u})$, where $k_{ij}^{n_v,n_u}=\int_\Omega\phi_i^{t_{n_v}}(\partial/\partial t\phi_j^{t_{n_u}})dX$.
- $\mathbf{f}^{n_v,n_f}=(f_i^{n_v,n_f})$ is right hand side vector, where $f_i^{n_v,n_f}=\int_\Omega\phi_i^{t_{n_v}}f^{t_{n_f}}dX$.

Here n_v, n_u, n_β, and n_f denote the time levels for the test function v, trial function u, coefficient function β, source function f, respectively.

The matrix $M_h^{n+1/2,n+1/2}+\frac{\tau}{2}A_h^{n+1/2,n+1/2,n+1/2}+\frac{\tau}{2}K_h^{n+1/2,n+1/2}$ is not symmetric since $K_h^{n+1/2,n+1/2}$ is not symmetric. However, a simplified algorithm has been proposed based on Theorem 3.1 in [37] and numerically illustrated to be optimally convergent in [37]:

$$\begin{aligned}&\left(M_h^{n+\frac12,n+\frac12}+\frac{\tau}{2}A_h^{n+\frac12,n+\frac12,n+\frac12}\right)\vec{u}^{n+1}\\ =&\left(M_h^{n+\frac12,n+\frac12}-\frac{\tau}{2}A_h^{n+\frac12,n+\frac12,n+\frac12}\right)\vec{u}^n+\tau\vec{f}^{n+\frac12,n+\frac12}.\end{aligned}\tag{3.13}$$

In this algorithm, the matrix $M_h^{n+1/2,n+1/2}+\frac{\tau}{2}A_h^{n+1/2,n+1/2,n+1/2}$ is symmetric positive definite matrix, which is critical to the AMG method. Then the IFE-AMG algorithm proposed above can be utilized to solve the linear system at each time iteration step with

$$\begin{aligned}A_h^1&=M_h^{n+\frac12,n+\frac12}+\frac{\tau}{2}A_h^{n+\frac12,n+\frac12,n+\frac12},\\ \vec{b}_h^1&=\left(M_h^{n+\frac12,n+\frac12}-\frac{\tau}{2}A_h^{n+\frac12,n+\frac12,n+\frac12}\right)\vec{u}^n+\tau\vec{f}^{n+\frac12,n+\frac12}.\end{aligned}$$

4 Numerical experiments

In this section, we present numerical examples to illustrate the features of bilinear and linear immersed finite element methods with algebraic multigrid solvers for both the stationary and moving interface problems. We set the initial vector u^0 to be 0 and the strong connection threshold $\eta = 0.25$. We denote number of V-cycles by V's, the size of the coarsest mesh by N_c, and the stopping tolerance on residual by tol. The Gauss-Seidel (GS) and incomplete LU (ILU) iterations are compared as the pre-smoothing and post-smoothing operations.

4.1 Numerical experiments for the steady interface problem

We consider the steady interface problem defined by (1.1)-(1.2b) on the typical rectangular domain $\Omega = [-1,1]\times[-1,1]$.

4.1.1 Circular interface

The interface curve Γ is a circle with radius $r_0 = \pi/6.28$ that separates Ω into two subdomains Ω^- and Ω^+ with $\Omega^- = \{(x,y)|x^2+y^2 \le r_0^2\}$. The coefficient function is

$$\beta(x,y) = \begin{cases} \beta^-, & (x,y)\in\Omega^-, \\ \beta^+, & (x,y)\in\Omega^+, \end{cases}$$

where $\beta^- = 1$ and $\beta^+ = 10$ are chosen in this example. The boundary condition function $g(x,y)$ and the source term $f(x,y)$ are chosen such that the following function u is the exact solution

$$u(x,y) = \begin{cases} \dfrac{r^\alpha}{\beta^-}, & \text{if } r \le r_0, \\ \dfrac{r^\alpha}{\beta^+} + \Big(\dfrac{1}{\beta^-} - \dfrac{1}{\beta^+}\Big) r_0^\alpha, & \text{otherwise}, \end{cases} \tag{4.1}$$

with $\alpha = 5$, $r = \sqrt{x^2+y^2}$. We use the bilinear immersed finite elements in this numerical experiment.

The errors of the IFE-AMG solutions with Gauss-Seidel smoother and various step size for small circular interface jump are given in Table 1. Using linear regression, we can also see that the errors in this table obey

$$\|u-u_h\|_{L^2} \approx 0.4229 h^{2.0022},$$
$$|u-u_h|_{H^1} \approx 0.8957 h^{0.9844}.$$

The errors of the IFE-AMG solutions with incomplete LU smoother and various step size for small interface are given in Table 2. Using linear regression, we can also see that the

Table 1: Errors of the bilinear IFE-AMG solution for the circular interface problem with GS smoother, $tol=10^{-8}$, $\beta^-/\beta^+=1/10$, and $\nu_1=\nu_2=2$.

h	N_c	$\|u-u_h\|_{L^2}$	$\|u-u_h\|_{H^1}$	$\|u-u_h\|_{l^\infty}$	V's
1/16	5^2	1.65383×10^{-3}	5.88161×10^{-2}	9.50035×10^{-4}	7
1/32	26^2	4.09991×10^{-4}	2.94836×10^{-2}	4.85435×10^{-4}	19
1/64	97^2	1.01487×10^{-4}	1.48173×10^{-2}	3.25996×10^{-4}	19
1/128	347^2	2.51954×10^{-5}	7.52028×10^{-3}	1.60087×10^{-4}	39
1/256	1235^2	6.46598×10^{-6}	3.84101×10^{-3}	7.68170×10^{-5}	130

Table 2: Errors of the bilinear IFE-AMG solution for the circular interface problem with ILU smoother, $tol=10^{-8}$, $\beta^-/\beta^+=1/10$, and $\nu_1=\nu_2=2$.

h	N_c	$\|u-u_h\|_{L^2}$	$\|u-u_h\|_{H^1}$	$\|u-u_h\|_{l^\infty}$	V's
1/16	5^2	1.65383×10^{-3}	5.88161×10^{-2}	9.50022×10^{-4}	1
1/32	26^2	4.10048×10^{-4}	2.94836×10^{-2}	4.85274×10^{-4}	2
1/64	97^2	1.01303×10^{-4}	1.48173×10^{-2}	3.26107×10^{-4}	2
1/128	347^2	2.51978×10^{-5}	7.52028×10^{-3}	1.59894×10^{-4}	5
1/256	1235^2	7.04174×10^{-6}	3.84099×10^{-3}	7.79246×10^{-5}	10

Table 3: Errors of the bilinear IFE-AMG solution for the circular interface problem with GS smoother, $tol=10^{-8}$, $\beta^-/\beta^+=1/10000$, and $\nu_1=\nu_2=2$.

h	N_c	$\|u-u_h\|_{L^2}$	$\|u-u_h\|_{H^1}$	$\|u-u_h\|_{l^\infty}$	V's
1/16	13^2	4.30316×10^{-4}	2.14209×10^{-2}	6.87757×10^{-4}	92
1/32	43^2	1.14524×10^{-4}	1.04928×10^{-2}	2.41457×10^{-4}	92
1/64	142^2	2.83999×10^{-5}	4.88765×10^{-3}	8.59457×10^{-5}	92
1/128	382^2	6.81981×10^{-6}	2.41970×10^{-3}	3.39365×10^{-5}	167
1/256	1327^2	1.57121×10^{-6}	1.21438×10^{-3}	1.77984×10^{-5}	170

errors in this table obey

$$\|u-u_h\|_{L^2}\approx 0.3882h^{1.9776},$$
$$|u-u_h|_{H^1}\approx 0.8957h^{0.9844}.$$

These linear regressions indicate that the bilinear IFE-AMG solutions with Gauss-Seidel or incomplete LU smoothers can converge with the optimal rates for small interface jump, which are second order in L^2 norm and first order in H^1 semi-norm.

The errors of the IFE-AMG solutions for large interface jump are given in Table 3. Using linear regression, we can also see that the errors in this table obey

$$\|u-u_h\|_{L^2}\approx 0.1245h^{2.0265},$$
$$|u-u_h|_{H^1}\approx 0.3801h^{1.0398},$$

which indicate that the bilinear IFE-AMG solutions can converge with the optimal rates for large interface jump.

Table 4: Number of V-cycles of the bilinear IFE-AMG solution for the circular interface problem with $tol=10^{-8}$.

	GS smoother			ILU smoother		
h	$\nu_1=\nu_2=1$	$\nu_1=\nu_2=2$	$\nu_1=\nu_2=3$	$\nu_1=\nu_2=1$	$\nu_1=\nu_2=2$	$\nu_1=\nu_2=3$
1/16	9	7	6	2	1	1
1/32	22	19	17	3	2	1
1/64	22	19	18	4	2	2
1/128	45	39	36	7	5	4
1/256	148	130	117	16	10	8

Table 5: Errors of the bilinear IFE-AMG solution for the circular interface problem with GS smoother, $tol=10^{-6}$, $\beta^-/\beta^+=1/10$, and $\nu_1=\nu_2=2$.

h	N_c	$\|u-u_h\|_{L^2}$	$\|u-u_h\|_{H^1}$	$\|u-u_h\|_{l^\infty}$	V's
1/16	5^2	1.65322×10^{-3}	5.88161×10^{-2}	9.51021×10^{-4}	5
1/32	26^2	4.03984×10^{-4}	2.94836×10^{-2}	5.03028×10^{-4}	12
1/64	97^2	9.35785×10^{-5}	1.48173×10^{-2}	3.56913×10^{-4}	12
1/128	347^2	6.39989×10^{-5}	7.52157×10^{-3}	2.28196×10^{-4}	36
1/256	1235^2	2.04489×10^{-4}	3.88786×10^{-3}	3.58655×10^{-4}	70

Table 6: Errors of the bilinear IFE-AMG solution for the circular interface problem with ILU smoother, $tol=10^{-6}$, $\beta^-/\beta^+=1/10$, and $\nu_1=\nu_2=2$.

h	N_c	$\|u-u_h\|_{L^2}$	$\|u-u_h\|_{H^1}$	$\|u-u_h\|_{l^\infty}$	V's
1/16	5^2	1.65383×10^{-3}	5.88161×10^{-2}	9.50022×10^{-4}	1
1/32	26^2	4.08628×10^{-4}	2.94836×10^{-2}	4.87086×10^{-4}	1
1/64	97^2	1.01303×10^{-4}	1.48173×10^{-2}	3.26107×10^{-4}	2
1/128	347^2	7.94820×10^{-5}	7.52023×10^{-3}	2.26107×10^{-4}	3
1/256	1235^2	2.18685×10^{-4}	3.87460×10^{-3}	2.67979×10^{-4}	70

The smoother usually has significant impact on the efficiency and accuracy of the solution. From Table 1 and Table 2, it can be also easily observed that the incomplete LU smoother significantly reduces the number of V-cycles, which dramatically improve the efficiency of the IFE-AMG method. Furthermore, from Table 4, we can also see that the increase of the number of smoothing steps may decrease the number of V-cycles while it increases the cost in smoothing phase. Hence the number of smoothing steps needs to be chosen properly in order to balance the total cost. The errors for the bilinear IFE-AMG solution with $\nu_1=\nu_2=1$ and $\nu_1=\nu_2=3$ are similar to those in Table 1 and Table 2. So we omit the corresponding data to shorten the presentation of the article.

In the following we will investigate the influence of the tolerance on the convergence of the IFE solutions for the interface problems. From Table 1 and Table 2, we can see that the bilinear IFE-AMG solutions with both Gauss-Seidel and incomplete LU smoothers converge in the optimal rates when $tol=10^{-8}$. However, from Table 5 and Table 6, we can see that when $tol=10^{-6}$ the bilinear IFE-AMG solutions do not perform optimally

any more. This indicates that the tolerance needs to be small enough for the chosen mesh size in order to keep the optimal convergence.

4.1.2 Elliptical interface

The interface curve Γ is an ellipse with its center at (x_0,y_0), whose major and minor radius are r_x, and r_y. The elliptical interface separates Ω into two sub-domains Ω^- and Ω^+ with $\Omega^- = \{(x,y)|(x-x_0)^2/r_x^2+(y-y_0)^2/r_y^2 \leq 1\}$ and we choose $x_0=0$, $y_0=0.2$, $r_x=3r_0/2$, $r_y=3r_0/4$, and $r_0=\pi/6.28$ in our numerical example. The coefficient function is

$$\beta(x,y)=\begin{cases} \beta^-, & (x,y)\in\Omega^-, \\ \beta^+, & (x,y)\in\Omega^+, \end{cases}$$

where $\beta^-=1$ and $\beta^+=10$ are chosen in this example. The boundary condition function $g(x,y)$ and the source term $f(x,y)$ are chosen such that the following function u is the exact solution.

$$u(x,y)=\begin{cases} \dfrac{1}{\beta^-}r_x^2r_y^2r^\alpha, & (x,y)\in\Omega^-, \\ \dfrac{1}{\beta^+}r_x^2r_y^2r^\alpha+\Big(\dfrac{1}{\beta^-}-\dfrac{1}{\beta^+}\Big)r_x^2r_y^2, & \text{otherwise}, \end{cases} \tag{4.2}$$

where $r=\sqrt{(x-x_0)^2/r_x^2+(y-y_0)^2/r_y^2}$ and $\alpha=5$. We use the linear immersed finite elements in this numerical experiment.

The errors of the IFE-AMG solutions with Gauss-Seidel smoother and various step size for small interface jump are given in Table 7. Using linear regression, we can also see that the errors in this table obey

$$\|u-u_h\|_{L^2}\approx 2.3084h^{1.9992},$$
$$|u-u_h|_{H^1}\approx 7.0284h^{0.9961}.$$

The errors of the IFE-AMG solutions with incomplete LU smoother and various step size for small interface are given in Table 8. Using linear regression, we can also see that the errors in this table obey

$$\|u-u_h\|_{L^2}\approx 2.3063h^{1.9989},$$
$$|u-u_h|_{H^1}\approx 7.0284h^{0.9961}.$$

These linear regressions indicate that the bilinear IFE-AMG solutions with Gauss-Seidel or incomplete LU smoothers can converge in the optimal rates, which are second order in L^2 norm and first order in H^1 semi-norm. Compared with the results of the above circular interface problem, We have similar observations for the influence of the smoother and tolerance on the convergence and efficiency. Hence we omit the corresponding data to shorten the presentation of the article.

Table 7: Errors of the linear IFE-AMG solution for the elliptical interface problem with GS smoother, $tol=10^{-8}$, $\beta^-/\beta^+=1/10$, and $\nu_1=\nu_2=2$.

h	N_c	$\|u-u_h\|_{L^2}$	$\|u-u_h\|_{H^1}$	$\|u-u_h\|_{l^\infty}$	V's
1/16	24^2	9.0180×10^{-3}	4.4409×10^{-1}	2.6189×10^{-3}	18
1/32	71^2	2.2670×10^{-3}	2.2268×10^{-1}	1.5906×10^{-3}	19
1/64	234^2	5.6605×10^{-4}	1.1162×10^{-1}	8.5101×10^{-4}	39
1/128	789^2	1.4123×10^{-4}	5.5972×10^{-2}	4.7140×10^{-4}	97

Table 8: Errors of the linear IFE-AMG solution for the elliptical interface problem with ILU smoother, $tol=10^{-8}$, $\beta^-/\beta^+=1/10$, and $\nu_1=\nu_2=2$.

h	N_c	$\|u-u_h\|_{L^2}$	$\|u-u_h\|_{H^1}$	$\|u-u_h\|_{l^\infty}$	V's
1/16	24^2	9.0180×10^{-3}	4.4409×10^{-1}	2.6189×10^{-3}	1
1/32	71^2	2.2670×10^{-3}	2.2268×10^{-1}	1.5906×10^{-3}	2
1/64	234^2	5.6632×10^{-4}	1.1162×10^{-1}	8.4960×10^{-4}	3
1/128	789^2	1.4131×10^{-4}	5.5972×10^{-2}	4.6736×10^{-4}	5

4.2 Numerical experiments for the moving interface problem

We consider the moving interface problem defined by (1.3)-(1.4b) on $\Omega\times[0,T_{end}]$, where $\Omega=(-1,1)\times(-1,1)$ and $T_{end}=1$. The interface $\Gamma(t)$ is a moving circle centered at origin with radius $r(t)$ which separates Ω into two sub-domains $\Omega^-(t)=\{(x,y)\in\Omega: x^2+y^2<r(t)^2\}$, and $\Omega^+(t)=\{(x,y)\in\Omega: x^2+y^2>r(t)^2\}$. Let $\beta^-=1$ and $\beta^+=10$. The exact solution is chosen as:

$$u(t,x,y)=\begin{cases}\dfrac{r^\alpha}{\beta^-}\cos(t), & r(t)\in\Omega^-(t),\\ \dfrac{r^\alpha}{\beta^+}\cos(t)+\Big(\dfrac{1}{\beta^-}-\dfrac{1}{\beta^+}\Big)r(t)^\alpha\cos(t), & r(t)\in\Omega^+(t).\end{cases}\tag{4.3}$$

In all the numerical examples presented below, the radius change is governed by $r(t)=r_0[(\sin(t)+3)/4]$ with $r_0=\pi/6.28$, and we use triangular Cartesian meshes $\mathcal{T}_h$ which are formed by partitioning Ω with $N_s\times N_s$ rectangles of size $h=2/N_s$ and then cutting each rectangle into two triangles along one of its diagonal line. For time discretization, we denote its step size by τ and define $t_n=n\tau$, with $n=1,2,\cdots,N$. We use the linear immersed finite elements in this numerical experiment.

The errors of the IFE-AMG solutions with Gauss-Seidel smoother and various step size are given in Table 9. Using linear regression, we can also see that the errors in this table obey

$$\|u-u_h\|_{L^2}\approx 0.6882h^{1.9381},$$
$$|u-u_h|_{H^1}\approx 0.6709h^{0.9234}.$$

The errors of the IFE-AMG solutions with incomplete LU smoother and various step size are given in Table 10. Using linear regression, we can also see that the errors in this table

Table 9: Errors of the linear IFE-AMG solution for the moving interface problem with GS smoother, $tol=10^{-8}$, and $\nu_1=\nu_2=2$ at time $t=T_{end}$.

h	N_c	$\|u-u_h\|_{L^2}$	$\|u-u_h\|_{H^1}$	$\|u-u_h\|_{l^\infty}$	V's
1/16	7^2	3.2659×10^{-3}	5.2764×10^{-2}	1.5801×10^{-3}	6
1/32	15^2	8.1519×10^{-4}	2.6920×10^{-2}	9.2506×10^{-4}	7
1/64	77^2	2.1175×10^{-4}	1.4116×10^{-2}	4.5706×10^{-4}	14
1/128	263^2	5.8132×10^{-5}	7.7486×10^{-3}	2.5078×10^{-4}	18

Table 10: Errors of the linear IFE-AMG solution for the moving interface problem with ILU smoother, $tol=10^{-8}$ and $\nu_1=\nu_2=2$ at time $t=T_{end}$.

h	N_c	$\|u-u_h\|_{L^2}$	$\|u-u_h\|_{H^1}$	$\|u-u_h\|_{l^\infty}$	V's
1/16	7^2	3.2659×10^{-3}	5.2764×10^{-2}	1.5801×10^{-3}	1
1/32	15^2	8.1519×10^{-4}	2.6920×10^{-2}	9.2506×10^{-4}	1
1/64	77^2	2.1175×10^{-4}	1.4116×10^{-2}	4.5711×10^{-4}	1
1/128	263^2	5.8122×10^{-5}	7.7486×10^{-3}	2.5078×10^{-4}	2

obey

$$\|u-u_h\|_{L^2}\approx 0.6883h^{1.9382},$$
$$|u-u_h|_{H^1}\approx 0.6709h^{0.9234}.$$

These linear regressions indicate that the linear IFE-AMG solutions with Gauss-Seidel or incomplete LU smoothers can converge in the optimal rates, which are second order in L^2 norm and first order in H^1 semi-norm. From Table 9 and Table 10, it can be also easily observed that the incomplete LU smoother significantly reduces the number of V-cycles, which dramatically improve the efficiency of the IFE-AMG method.

It is also clearly showed in Fig. 5 that the algebraic multigrid solver is stable and effi-

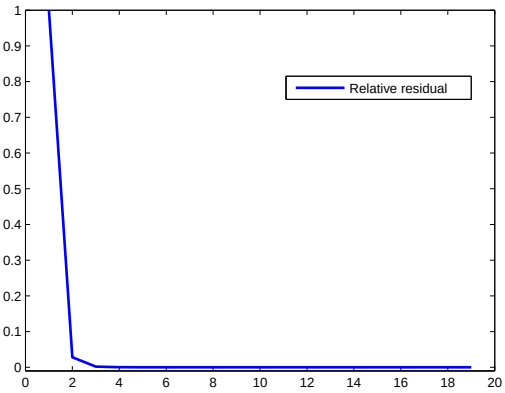

Figure 5: Relative residual of the iterations at $t=1$ for the linear IFE-AMG solution with $h=1/128$, GS smoother, $tol=10^{-8}$, and $(\nu_1,\nu_2)=(2,2)$.

Table 11: Number of V-cycles of the linear IFE-AMG solution at different time steps for the moving interface problem with GS smoother and $tol=10^{-8}$.

h	$t=\Delta t$	$t=\frac{1}{4}$	$t=\frac{1}{2}$	$t=\frac{3}{4}$	$t=1$
1/32	8	8	13	8	7
1/64	8	8	12	8	14
1/128	9	13	19	15	18

Table 12: Number of V-cycles of the linear IFE-AMG solution at different time steps for the moving interface problem with ILU smoother and $tol=10^{-8}$.

h	$t=\Delta t$	$t=\frac{1}{4}$	$t=\frac{1}{2}$	$t=\frac{3}{4}$	$t=1$
1/32	1	1	1	1	1
1/64	1	1	1	1	1
1/128	1	2	2	2	2

cient for the linear systems arising from the IFE methods since the residual error quickly decreases to a small magnitude.

Furthermore, Tables 11 and 12 provide the number of V-cycles of the linear IFE-AMG solution at different time steps when the interface locations are different. We observe that the number of V-cycles for Gauss-Seidel smoother depend on the moving interface locations but not very severely. The incomplete LU smoother may reduce the dependence of the number of V-cycles on the moving interface since it needs much less number of V-cycles than the Gauss-Seidel smoother.

5 Conclusions

In this article, we discussed the bilinear and linear immersed finite element (IFE) solutions generated from the algebraic multigrid solver for both stationary and moving interface problems. The feature of the symmetric positive-definite matrices from the IFE methods naturally matches the corresponding need of the algebraic multigrid solver in order to guarantee its efficiency. Furthermore, the combination of other features of the algebraic multigrid method and the IFE methods, such as the preconditioning property, the optimal convergence rates, and the flexibility to handle the interface on structured meshes instead of body-fitting meshes, can dramatically improve the efficiency of the proposed methods when the IFE-AMG method is applied to real world applications. Numerical experiments are performed to demonstrate these features as well as the influence of the tolerance and the smoother on the efficiency and convergence.

Acknowledgments

This work is partially supported by DOE grant DE-FE0009843, National Natural Science Foundation of China (11175052), GRF of HKSAR #501012 and NSERC (Canada).

References

[1] S. Adjerid and T. Lin, Higher-order immersed discontinuous Galerkin methods, Int. J. Inf. Syst. Sci., 3(4) (2007), 555–568.

[2] S. Adjerid and T. Lin, p-th degree immersed finite element for boundary value problems with discontinuous coefficients, Appl. Numer. Math, 59(6) (2009), 1303–1321.

[3] A. Almgre, J. B. Bell, P. Collela, and T. Marthaler, A cartesian grid emthod for imcompressible Euler equations in complex geometries, SIAM J. Sci. Comput., 18 (1997), 1289–1390.

[4] Y. Arakawa and M. Nakano, An efficient three-dimensional optics code for ion thruster research, In AIAA-3196, 1996.

[5] I. Babuška, The finite element method for elliptic equations with discontinuous coefficients, Computing, 5 (1970), 207–213.

[6] I. Babuška and J. E. Osborn, Can a finite element method perform arbitrarily badly?, Math. Comput., 69(230) (2000), 443–462.

[7] M. P. Bendsøe and N. Kikuchi, Generating optimal topologies in optimal design using a homogenization method, Comput. Meth. Appl. Mech. Eng., 71 (1988), 197–224.

[8] I. Boyd, D. VanGilde, and X. Liu, Monte carlo simulation of neutral xenon flows in electric propulsion devices, J. Propulsion Power, 14(6) (1998), 1009–1015.

[9] J. H. Bramble and J. T. King, A finite element method for interface problems in domains with smooth boundary and interfaces, Adv. Comput. Math., 6 (1996), 109–138.

[10] B. Camp, T. Lin, Y. Lin, and W. Sun, Quadratic immersed finite element spaces and their approximation capabilities, Adv. Comput. Math., 24(1-4) (2006), 81–112.

[11] J. R. Cannon, Jr. Douglas, Jim, and C. Denson Hill, A multi-boundary stefan problem and the disappearance of phases, J. Math. Mech., 17 (1967), 21–33.

[12] Q. Chang, Y. Wong, and H. Fu, On the algebraic multigrid method, J. Comput. Phys., 125 (1996), 279–292.

[13] T. Chen and J. Strain, Piecewise-polynomial discretization and Krylov-accelerated multigrid for elliptic interface problems, J. Comput. Phys., 227 (2008), 7503–7542.

[14] Z. Chen and J. Zou, Finite element methods and their convergence for elliptic and parabolic interface problems, Numer. Math., 79 (1998), 175–202.

[15] A. J. Chorin, A numerical method for solving incompressible viscous flow problems, J. Comput. Phys., 2 (1967), 12.

[16] S. Chou, An immersed linear finite element method with interface flux capturing recovery, Discrete Contin. Dyn. Syst. Ser. B, 17(7) (2012), 2343–2357.

[17] S. Chou, D. Y. Kwak, and K. T. Wee, Optimal convergence analysis of an immersed interface finite element method, Adv. Comput. Math., 33(2) (2010), 149–168.

[18] Y. Chu, Y. Cao, X.-M. He, and M. Luo, Asymptotic boundary conditions for two-dimensional electrostatic field problems with immersed finite elements, Comput. Phys. Commun., 182(11) (2011), 2331–2338.

[19] A. Dadone and B. Grossman, Design optimization of fluid dynamic problems using cartesian grids, In K. Srinivas, S. Armfield and P. Morgan, editor, Computational Fluid Dynamics 2002, Verlin, 591–596, Springer.

[20] R. E. Ewing, Z. Li, T. Lin, and Y. Lin, The immersed finite volume element methods for the elliptic interface problems, Modelling '98 (prague), Math. Comput. Simul., 50(1-4) (1999), 63–76.

[21] X. Feng and Z. Li, Simplified immersed interface methods for elliptic interface problems with straight interfaces, Numer. Methods Partial Differential Equations, 28(1) (2012), 188–

203.
[22] X. Feng, Z. Li, and L. Wang, Analysis and numerical methods for some crack problems, Int. J. Numer. Anal. Model. Ser. B, 2(2-3) (2011), 155–166.
[23] A. L. Fogelson and J. P. Keener, Immersed interface methods for Neumann and related problems in two and three dimensions, SIAM J. Sci. Comput., 22 (2001), 1630–1654.
[24] W. Geng and G. W. Wei, Multiscale molecular dynamics using the matched interface and boundary method, J. Comput. Phys., 230(2) (2011), 435–457.
[25] B. H. Gilding, Qualitative mathematical analysis of the Richards equation, Transport Porous Med., 6(5-6) (1991), 651–666.
[26] Y. Gong, B. Li, and Z. Li, Immersed-interface finite-element methods for elliptic interface problems with non-homogeneous jump conditions, SIAM J. Numer. Anal., 46 (2008), 472–495.
[27] Y. Gong and Z. Li, Immersed interface finite element methods for elasticity interface problems with non-homogeneous jump conditions, Numer. Math. Theory Methods Appl., 3(1) (2010), 23–39.
[28] B. E. Griffith and S. Lim, Simulating an elastic ring with bend and twist by an adaptive generalized immersed boundary method, Commun. Comput. Phys., 12(2) (2012), 433–461.
[29] R. D. Guy and B. Philip, A multigrid method for a model of the implicit immersed boundary equations, Commun. Comput. Phys., 12(2) (2012), 378–400.
[30] X.-M. He, Bilinear Immersed Finite Elements for Interface Problems, Ph.D. dissertation, Virginia Polytechnic Institute and State University, 2009.
[31] X.-M. He, T. Lin, and Y. Lin, Approximation capability of a bilinear immersed finite element space, Numer. Methods Partial Differential Equations, 24(5) (2008), 1265–1300.
[32] X.-M. He, T. Lin, and Y. Lin, A bilinear immersed finite volume element method for the diffusion equation with discontinuous coefficients, Commun. Comput. Phys., 6(1) (2009), 185–202.
[33] X.-M. He, T. Lin, and Y. Lin, Interior penalty discontinuous Galerkin methods with bilinear IFE for a second order elliptic equation with discontinuous coefficient, dedicated to Professor David Russell's 70th birthday, J. Syst. Sci. Complex., 23(3) (2010), 467–483.
[34] X.-M. He, T. Lin, and Y. Lin, Immersed finite element methods for elliptic interface problems with non-homogeneous jump conditions, Int. J. Numer. Anal. Model., 8(2) (2011), 284–301.
[35] X.-M. He, T. Lin, and Y. Lin, The convergence of the bilinear and linear immersed finite element solutions to interface problems, Numer. Methods Partial Differential Equations, 28(1) (2012), 312–330.
[36] X.-M. He, T. Lin, and Y. Lin, A selective immersed discontinuous Galerkin method for elliptic interface problems, Math. Methods Appl. Sci., 2013, accepted.
[37] X.-M. He, T. Lin, Y. Lin, and X. Zhang, Immersed finite element methods for parabolic equations with moving interface, Numer. Methods Partial Differential Equations, 29(2) (2013), 619–646.
[38] B. Heinrich, Finite Difference Methods on Irregular Networks, volume 82 of Int. Series Numer. Math., Birkhäuser, Boston, 1987.
[39] D. W. Hewitt, The embedded curved boundary method for orthogonal simulation meshes, J. Comput. Phys., 138 (1997), 585–616.
[40] D. M. Ingram, D. M. Causon, and C. G. Mingham, Developments in Cartesian cut cell methods, Math. Comput. Simul., 61(3-6) (2003), 561–572.
[41] H. Ji, F.-S. Lien, and E. Yee, An efficient second-order accurate cut-cell method for solving the variable coeffcient Poisson equation with jump conditions on irregular domains, Int. J.

Numer. Methods Fluids, 52 (2006), 723–748.
[42] H. Johansen and P. Colella, A Cartesian grid embedded boundary method for Poisson's equation on irregular domains, J. Comput. Phys., 147 (1998), 60–85.
[43] R. Kafafy, T. Lin, Y. Lin, and J. Wang, Three-dimensional immersed finite element methods for electric field simulation in composite materials, Int. J. Numer. Meth. Eng., 64(7) (2005), 940–972.
[44] R. Kafafy, J. Wang, and T. Lin, A hybrid-grid immersed-finite-element particle-in-cell simulation model of ion optics plasma dynamics, Dyn. Contin. Discrete Impuls. Syst. Ser. B Appl. Algorithms, 12 (2005), 1–16.
[45] Y. Kim, Y. Seol, M. Lai, and C. S. Peskin, The immersed boundary method for two-dimensional foam with topological changes, Commun. Comput. Phys., 12(2) (2012), 479–493.
[46] D. Y. Kwak, K. T. Wee, and K. S. Chang, An analysis of a broken p_1-nonconforming finite element method for interface problems, SIAM J. Numer. Anal., 48(6) (2010), 2117–2134.
[47] T. P. Chartier and L. Adams, New geometric immersed interface multigrid solvers, SIAM J. Sci. Comput., 25(5) (2004), 1516–1533.
[48] T. P. Chartier and L. Adams, A comparison of algebraic multigrid and geometric immersed interface multigrid methods for interface problems, SIAM J. Sci. Comput., 26(3) (2005), 762–784.
[49] Z. Li and L. Adams, The immersed interface/multigrid methods for interface problems, SIAM J. Sci. Comput., 24(2) (2002), 463–479.
[50] R. J. LeVeque and Z. Li, The immersed interface method for elliptic equations with discontinuous coefficients and singular sources, SIAM J. Numer. Anal., 34 (1994), 1019–1044.
[51] Z. Li, The immersed interface method using a finite element formulation, Appl. Numer. Math., 27(3) (1997), 253–267.
[52] Z. Li and K. Ito, The immersed interface method: Numerical solutions of PDEs involving interfaces and irregular domains, volume 33 of Frontiers in Applied Mathematics, Society for Industrial and Applied Mathematics (SIAM), Philadelphia, PA, 2006.
[53] Z. Li, T. Lin, Y. Lin, and R. C. Rogers, An immersed finite element space and its approximation capability, Numer. Methods Partial Differential Equations, 20(3) (2004), 338–367.
[54] Z. Li, T. Lin, and X. Wu, New Cartesian grid methods for interface problems using the finite element formulation, Numer. Math., 96(1) (2003), 61–98.
[55] Z. Li and P. Song, An adaptive mesh refinement strategy for immersed boundary/interface methods, Commun. Comput. Phys., 12(2) (2012), 515–527.
[56] T. Lin, Y. Lin, R. C. Rogers, and L. M. Ryan, A rectangular immersed finite element method for interface problems, In P. Minev and Y. Lin, editors, Advances in Computation: Theory and Practice, Vol. 7, 107–114. Nova Science Publishers, Inc., 2001.
[57] T. Lin, Y. Lin, and W. Sun, Error estimation of a class of quadratic immersed finite element methods for elliptic interface problems, Discrete Contin. Dyn. Syst. Ser. B, 7(4) (2007), 807–823.
[58] T. Lin, Y. Lin, W. Sun, and Z. Wang, Immersed finite element methods for 4th order differential equations, J. Comput. Appl. Math., 235(13) (2011), 3953–3964.
[59] T. Lin and D. Sheen, The immersed finite element method for parabolic problems with the Laplace transformation in time discretization, Int. J. Numer. Anal. Model., 10(2) (2013), 298–313.
[60] T. Lin and J. Wang, An immersed finite element electric field solver for ion optics modeling, In Proceedings of AIAA Joint Propulsion Conference, Indianapolis, IN, July, 2002. AIAA,

2002-4263.
[61] T. Lin and J. Wang, The immersed finite element method for plasma particle simulation, In Proceedings of AIAA Aerospace Sciences Meeting, Reno, NV, Jan., 2003, AIAA, 2003-0842.
[62] G. H. Meyer, Multidimensional stefan problems, SIAM J. Numer. Anal., 10 (1973), 522–538.
[63] C. S. Peskin, Flow patterns around heart valves, J. Comput. Phys., 10 (1972), 252–271.
[64] C. S. Peskin, Numerical analysis of blood flow in the heart, J. Comput. Phys., 25 (1977), 220–252.
[65] J. W. Ruge and K. Stüben, Algebraic multigrid, In S. F. McCormick, editor, Multigrid methods, SIAM, Philadelphia, 4 (1987), 73–130.
[66] S. A. Sauter and R. Warnke, Composite finite elements for elliptic boundary value problems with discontinuous coefficients, Computing, 77(1) (2006), 29–55.
[67] K. Stüben, Algebraic multigrid (AMG): experiences and comparisons, Appl. Math. Comput., 13 (1983), 419–451.
[68] Z. Tan, D. V. Le, K. M. Lim, and B. C. Khoo, An immersed interface method for the simulation of inextensible interfaces in viscous fluids, Commun. Comput. Phys., 11(3) (2012), 925–950.
[69] C. Oosterlee U. Trottenberg and A. Schuller, Multigrid, volume 631, Academic Press, London, 2001.
[70] S. Vallaghè and T. Papadopoulo, A trilinear immersed finite element method for solving the electroencephalography forward problem, SIAM J. Sci. Comput., 32(4) (2010), 2379–2394.
[71] J. Wang, X.-M. He, and Y. Cao, Modeling spacecraft charging and charged dust particle interactions on lunar surface, Proceedings of the 10th Spacecraft Charging Technology Conference, Biarritz, France, 2007.
[72] J. Wang, X.-M. He, and Y. Cao, Modeling electrostatic levitation of dusts on lunar surface, IEEE Trans. Plasma Sci., 36(5) (2008), 2459–2466.
[73] K. Wang, H. Wang, and X. Yu, An immersed eulerian-lagrangian localized adjoint method for transient advection-diffusion equations with interfaces, Int. J. Numer. Anal. Model., 9(1) (2012), 29–42.
[74] C. Wu, Z. Li, and M. Lai, Adaptive mesh refinement for elliptic interface problems using the non-conforming immersed finite element method, Int. J. Numer. Anal. Model., 8(3) (2011), 466–483.
[75] H. Xie, Z. Li, and Z. Qiao, A finite element method for elasticity interface problems with locally modified triangulations, Int. J. Numer. Anal. Model., 8(2) (2011), 189–200.
[76] S. Xu, An iterative two-fluid pressure solver based on the immersed interface method, Commun. Comput. Phys., 12(2) (2012), 528–543.
[77] M. Ye, R. Khaleel, and T. J. Yeh, Stochastic analysis of moisture plume dynamics of a field injection experiment, Water Resour. Res., 41 (2005), W03013.
[78] S. Zhao, High order matched interface and boundary methods for the Helmholtz equation in media with arbitrarily curved interfaces, J. Comput. Phys., 229(9) (2010), 3155–3170.
[79] Y. C. Zhou, J. Liu, and D. L. Harry, A matched interface and boundary method for solving multi-flow Navier-Stokes equations with applications to geodynamics, J. Comput. Phys., 231(1) (2012), 223–242.
[80] Y. C. Zhou and G. W. Wei, On the fictitious-domain and interpolation formulations of the matched interface and boundary (MIB) method, J. Comput. Phys., 219(1) (2006), 228–246.
[81] Y. C. Zhou, S. Zhao, M. Feig, and G. W. Wei, High order matched interface and boundary method for elliptic equations with discontinuous coefficients and singular sources, J. Comput. Phys, 213(1) (2006), 1–30.